Max-Planck-Institut
für Meteorologie

REPORT No. 227

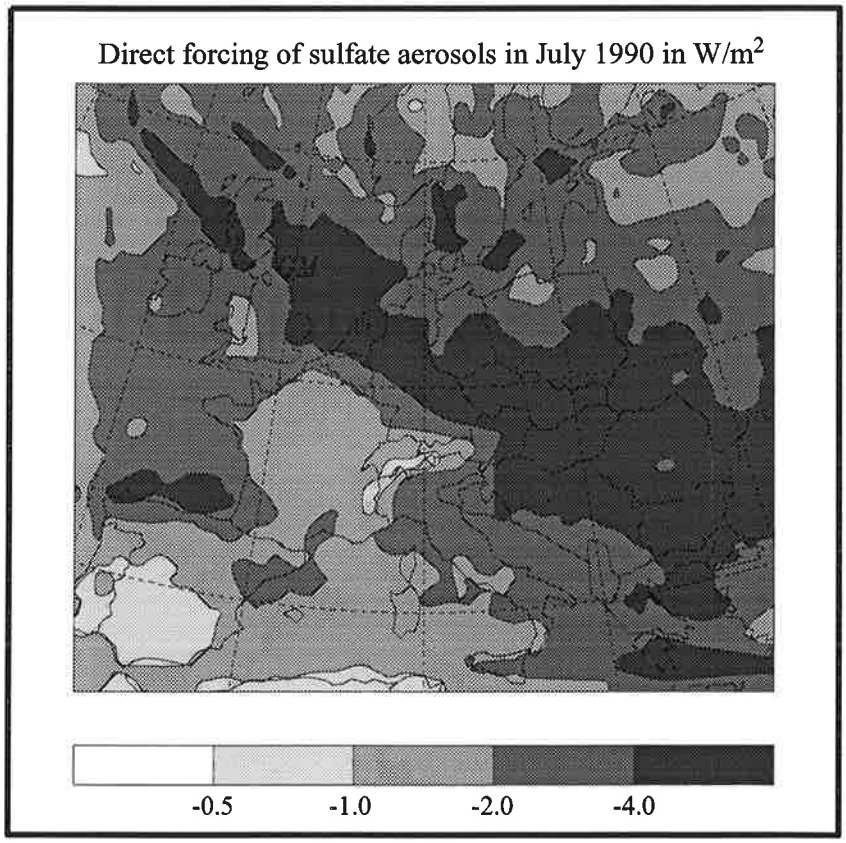

RADIATIVE FORCING OF SULFATE AEROSOLS AS DETERMINED BY A REGIONAL CIRCULATION-CHEMISTRY TRANSPORT MODEL

by

Bärbel Langmann · Michael Herzog · Hans-F. Graf

HAMBURG, January 1997

AUTHORS:

Bärbel Langmann
Michael Herzog
Hans-F. Graf

Max-Planck-Institut
für Meteorologie

MAX-PLANCK-INSTITUT
FÜR METEOROLOGIE
BUNDESSTRASSE 55
D - 20146 HAMBURG
GERMANY

Tel.: +49-(0)40-4 11 73-0
Telefax: +49-(0)40-4 11 73-298
E-Mail: <name> @ dkrz.de

ISSN 0937-1060

Radiative Forcing of Sulfate Aerosols as determined by a regional Circulation-Chemistry Transport Model

Bärbel Langmann, Michael Herzog and Hans-F. Graf

Max Planck Institute for Meteorology
Bundesstr. 55, D-20146 Hamburg, Germany

Abstract

Besides their acidifying effect, H_2SO_4 / SO_4^{2-} aerosols have the potential to modify the radiation budget of the atmosphere. Under clear-sky condition they scatter UV-radiation back to space, reducing solar irradiance (direct effect). The capability of sulfate particles to act as cloud condensation nuclei, thus influencing cloud droplet number concentration, cloud albedo and the development of precipitation is referred to as indirect effect. Evidence has been presented that sulfate aerosol climate forcing is sufficiently large to reduce significantly the positive forcing by anthropogenic greenhouse gases regionally, especially in the Northern Hemisphere.

Until now, only coarse grid global models with rather simple chemistry modules have been applied to estimate the radiative forcing of sulfate aerosols. In this paper we would like to ascertain the shortwave sulfate forcing over Europe, one of the main anthropogenic source regions. For this purpose the three-dimensional European sulfate distribution was generated by a regional circulation model in combination with a complex chemistry transport model. Then a computationally efficient radiation transfer model was applied. It determines the direct and indirect shortwave forcing of sulfate aerosols on the basis of the variable sulfate mass distribution and meteorological input data. For comparison coarse grid global model results will be shown.

Radiative Forcing of Sulfate Aerosols as determined by a regional Circulation-Chemistry Transport Model

Bärbel Langmann, Michael Herzog and Hans-F. Graf

Max Planck Institute for Meteorology
Bundesstr. 55, D-20146 Hamburg, Germany

1. Introduction

Searching for anthropogenic climate change signals, recently the role of sulfate aerosols was emphasized by Charlson et al. (1991) and Kiehl and Briegleb (1993). Following these papers, several groups tried to estimate the contribution of anthropogenic sulfur emissions in reducing the global climate signal due to the increased greenhouse gas concentration in the atmosphere (Wigley et al., 1990; Taylor and Penner, 1994; Roeckner et al., 1995; Mitchell et al., 1995). Other groups tried to improve knowledge of the necessary optical parameters of the aerosols applying radiative transfer models to aerosol-box models (Pilinis et al., 1995; Nemesure et al., 1995) or to global models (Boucher and Anderson, 1995; and Boucher and Lohmann, 1995). Thus, either the aerosol and its changing parameters due to microphysical processes or large-scale mean parameters were studied so far. These investigations revealed that one of the most important aerosol parameters is its size distribution which mainly depends on the relative humidity of the surrounding air.

None of the models, however, treated the inhomogeneity of the aerosol forcing in one of the continental scale source regions of anthropogenic sulfate aerosols. While Boucher and Anderson (1995) used the MOGUNTIA model with 10° resolution, Boucher and Lohmann (1995) in addition to the latter used the spectral ECHAM3 model with T21 truncation, which gives a 5.6° resolution, comparable with the French LMD gridpoint model. The very simple approach of Roeckner et al. (1995) and Mitchell et al. (1995), who, in order to describe the sulfate aerosol effect, just changed the surface albedo depending on the sulfate concentration as computed with a simple sulfur cycle model, may be useful for a first guess of the effects. However, the possible patchiness of the forcing is neglected as well as the indirect effects and the impact of local air humidity and cloud cover. Despite their simpleness in describing the aerosol forcing, these model studies allowed to improve the guess patterns of the anthropogenic greenhouse gas climate anomalies such that a better agreement between observed and modelled change patterns was achieved. This allowed to a high degree of certainty the assessment of the observed changes in surface air temperature to anthropogenic impact (Hasselmann et al., 1995; IPCC, 1996).

While the above mentioned model simulation in the best case had a T42 (or 250 km) resolution, the sources and regional circulation systems in the main anthropogenic source regions of volatile sulfur have smaller length scales. In the coarse resolution models the chemistry has to be treated in a rather simple manner, since many of the chemical transformations for these models take place in the sub-grid domain and are, therefore, parameterized. This leads also to rather homogeneous forcing fields. Since the sources are not equally distributed over areas of more than 60 000 km^2, but concentrate in areas of industrial development in the neighbourhood of agriculturally used land, it is interesting to study what happens in the smaller domain.

With our study we shall try to resolve these effects of nonhomogeneously distributed sources of sulfate aerosol precursor gases. Therefore we use a combination of the Hamburg regional circulation model HIRHAM with an improved version (Langmann, 1995) of the EURAD chemis-

try transport model (Hass, 1991). The advantage of this model configuration is that e.g. cloud water is a prognostic variable. This helped to improve the sulfur chemistry as compared with the EURAD version. Sensitivity studies and a comparison of the model results for one winter and one summer episode have been published (Langmann and Graf, 1996). The resolution of the model is 0.5°, and it covers the Atlantic/Europe area. The chemistry module based on RADM II (Stockwell et al., 1990) goes well beyond what was used so far in GCM simulations. A short description of this model configuration is given in section 2.

A very fast, optimized version of a radiative transfer model was used as an off-line analysis tool. This tool allows for a much more detailed investigation of the shortwave radiative forcing than does the HIRHAM or ECHAM standard radiation code. The radiative transfer depends on the local distribution of sulfate aerosols and their main optically relevant properties. With this approach also the effect of the relative humidity will be studied, which, based on the higher resolution of the circulation model, allows also a better consideration of the covariance of the sulfate and humidity fields. The radiative analysis tool is presented in section 3.

In section 4 two episodes (one for winter and one for summer) are studied for their local and large scale radiative effects. To ascertain the shortwave sulfate forcing on the European scale, results from a coarse resolution global model simulation (Graf et al., 1996) with simplified chemistry are compared to results from the regional model simulation. Section 5 summarizes the results and conclusions are given.

2. Description of the regional model system

A combination of the regional circulation model HIRHAM (Kållberg, 1989) with a modified version (Langmann, 1995) of the EURAD Chemistry-Transport-Model (CTM) (Hass, 1991) for the polluted atmosphere was applied. The meteorological driver model HIRHAM produces information about the physical conditions of the atmosphere (horizontal wind, temperature, specific moisture, liquid water content, surface pressure, cloud cover and precipitation), which are passed to the CTM. Transport, dry and wet deposition, production and loss of chemical species are then determined by the CTM. The horizontal resolution is 0.5° on a spherical rotated grid. In the vertical a terrain following hybrid pressure sigma-coordinate system with 19 layers of unequal thickness between the ground and the 10 hPa pressure level is applied. The model area covers Europe, except the northern parts of Scandinavia.

Horizontal and vertical advection are determined by the scheme of Smolarkiewitz (1983). The subgrid-scale turbulent transport in the planetary boundary layer follows a parameterization based on scaling regimes as described by Hass (1991). For the treatment of dry deposition an approach derived by Wesely (1989) is used. The complex tropospheric gas-phase chemistry package (158 chemical reactions between 60 species) is described by Stockwell et al. (1990). Aqueous chemistry processes are calculated with cloud mean values from cloud base to cloud top. The determination of cloud boundaries and the vertical redistribution of chemical species in clouds is based on an approach proposed by Mölders and Laube (1994).

Clear sky photolysis rates for 21 photolysis reactions are created by a climatological preprocessor model (Madronich, 1987). If clouds appear in a grid box, photolysis rates are modified according to Chang et al. (1987). Emission data are provided on the basis of Memmesheimer et al. (1991). In the current model version estimated vertical concentration profiles of a relatively unpolluted atmosphere are used as initial and boundary condition. Two days prior to the simulation period, an initialization run is started with these horizontally uniform, vertically varying clean conditions plus realistic meteorology and emissions.

3 Radiation Model

The radiation code for the solar spectrum applied in the fourth generation general circulation model ECHAM (Roeckner et al., 1996) and the regional circulation model HIRHAM uses a two stream method based on Fouquart and Bonnel (1980). The solar spectrum is divided into two bands only. Rayleigh scattering is included via a parametric expression of optical thickness. Therefore it is difficult to regard additional scatterers like aerosols in a straight forward manner. Especially the use of two broad bands requires an averaging over spectral intervalls with highly variable optical properties for aerosols. The delta-Eddington approximation avoids the problem of parametrizing scattering effects because it includes single as well as multiple scattering. The introduction of more spectral intervalls reduces the problem of the averaging procedure.

Here we present a very efficient and computationally fast method of the delta-Eddington approximation for a multi layer atmosphere. This method requires neglectable restrictions on the allowed optical properties to guarantee stability of the scheme.

3.1 The delta-Eddington approximation

The delta-Eddington approximation leads to an analytical solution of the monochromatic radiative transfer equation

$$\begin{aligned}
\mu\frac{d}{d\tau}I(\tau,\mu,\phi) \;=\; & -I(\tau,\mu,\phi) && \text{extinction}\\
& +\frac{\omega(\tau)}{4\pi}\int_{-1}^{+1} P(\mu,\phi,\mu',\phi')I(\tau,\mu',\phi')d\mu'd\phi' && \text{multiple scattering}\\
& +\frac{\omega(\tau)}{4\pi}(\pi F_0)e^{-\tau/\mu_0}P(\mu,\phi,\mu_0,\phi_0) && \text{single scattered solar radiation}\\
& +(1-\omega(\tau))B(T) && \text{Planck radiation}
\end{aligned} \tag{1}$$

where the following notation is used:

$I(\tau,\mu,\phi)$	diffuse radiance
$\tau = \int_0^z \sigma_{ext}(z')dz'$	optical depth
σ_{ext}	extinction coefficient
$\mu = cos\vartheta$	ϑ zenith angle
ϕ	azimuth angle
$P(\mu,\phi,\mu',\phi')$	phase function
$\omega(\tau) = \sigma_{sca}/\sigma_{ext}$	single scattering albedo
σ_{sca}	scattering coefficient
πF_0	solar irradiance

If the radiance I is known, the diffuse upward and downward fluxes can easily be computed. Eddington's approximation assumes that the radiance can be approximated by a first order Legendre polynomial:

$$I(\tau,\mu,\phi) = I_0(\tau) + \mu I_1(\tau) \tag{2}$$

Because the radiance is set independent of ϕ, this approximation can be valid only for horizontally homogeneous atmospheres. Furthermore the Eddington approximation belongs to the two stream approximations. From eqs. (1) and (2) we can conclude that the phase function must be of the form:

$$P(\mu, \phi, \mu', \phi') = P(\theta) = 1 + 3g(\tau)cos\theta \tag{3}$$

The angle θ is the angle between the incident and scattered directions $\Omega = (\mu, \phi)$ and $\Omega' = (\mu', \phi')$:

$$cos\theta = \mu\mu' + \sqrt{1-\mu^2}\sqrt{1-\mu'^2}\, cos(\phi - \phi')$$

The asymmetry factor g is the first moment of the original phase function:

$$g(\tau) = \frac{1}{2}\int_{-1}^{+1} P(\theta)cos\theta\, dcos\theta$$

The combination of eqs. (1), (2) and (3) results in a strongly simplified radiative transfer equation:

$$\begin{aligned} \mu\frac{d}{d\tau}(I_0 + \mu I_1) &= -(I_0 + \mu I_1) \\ &\quad +\omega(I_0 + g\mu I_1) \\ &\quad +\frac{\omega}{4\pi}(\pi F_0)e^{-\tau/\mu_0} \\ &\quad +(1-\omega)B \end{aligned} \tag{4}$$

By applying $\int_{-1}^{+1} d\mu$ and $\int_{-1}^{+1} \mu d\mu$ to eq.(4) we obtain a pair of coupled ordinary differential equations,

$$\frac{d}{d\tau}I_1 = -3(1-\omega)I_0 + \frac{3}{4\pi}\omega(\pi F_0)e^{-\tau/\mu_0} + 3(1-\omega)B \tag{5}$$

$$\frac{d}{d\tau}I_0 = -(1-\omega g)I_1 + \frac{3}{4\pi}\omega g(\pi F_0)e^{-\tau/\mu_0} \tag{6}$$

In general it is not possible to find analytical solutions to eqs. (5) and (6). But in the special case of a vertical homogeneous atmosphere or atmospheric layer, where

$$\begin{aligned} \frac{d}{d\tau}g &= 0 \\ \frac{d}{d\tau}\omega &= 0 \\ \frac{d}{d\tau}B &= const, \end{aligned} \tag{7}$$

the analytical solution is given by

$$\begin{aligned} \pi I_0(\tau) &= c_1 e^{-k\tau} + c_2 e^{k\tau} - \alpha e^{-\tau/\mu_0} + \pi B(\tau) \\ \frac{2}{3}\pi I_1(\tau) &= p(c_1 e^{-k\tau} - c_2 e^{k\tau}) - \beta e^{-\tau/\mu_0} - \frac{2\pi}{3(1-\omega g)}\frac{\partial B}{\partial \tau} \end{aligned} \tag{8}$$

where

$$\begin{aligned} k &= \sqrt{3(1-\omega)(1-\omega g)} \\ p &= \frac{2}{3}\sqrt{3(1-\omega)/(1-\omega g)} \\ \alpha &= \frac{3}{4}(\pi F_0)\omega\mu_0^2\frac{1+g(1-\omega)}{1-k^2\mu^2} \\ \beta &= \frac{1}{2}(\pi F_0)\omega\mu_0\frac{1+3g\mu_0^2(1-\omega)}{1-k^2\mu^2} \end{aligned} \tag{9}$$

with the restrictions

$$\omega \neq 1 \tag{10}$$
$$\mu_0 \neq 1/k, \tag{11}$$

c_1 and c_2 are given by boundary conditions. The restriction in eq. (10) means that the derived solution does not describe the case of pure scattering. For real atmospheric conditions this is always true. Equation (11) is not a substantial restriction because the solution (8) approaches a finite limit as $\mu_0 \to 1/k$.

In the delta-Eddington approximation the phase function is extended by a Dirac delta function:

$$P(\theta) = 2f\delta(1 - cos\theta) + (1 - f)(1 + 3g'cos\theta) \tag{12}$$

where:

$f = g^2$	fractional scattering into the forward direction
$g' = g/(1 + g)$	scaled asymmetry factor

The delta function allows to describe an additional forward scatter peak and enables the use of a more realistic phase function. In the case of highly asymmetric phase functions the delta-Eddington approximation is a substantial improvement compared with the original Eddington approximation. The solution of eq. (1) for the delta-Eddington approximation is also given by eqs. (8) by replacing the optical properties τ, g and ω with the scaled quantities:

$$\begin{aligned} \tau' &= (1 - \omega g^2)\tau \\ g' &= \frac{g}{1+g} \\ \omega' &= \frac{1+g^2}{1-\omega g^2}\omega \end{aligned}$$

Thus Eddington and delta-Eddington approximation are formally equivalent.

Using the solution in eqs. (8) the diffuse and the net fluxes are given by:

$$\begin{aligned} F^{\downarrow,\uparrow}(\tau) &= \pi(I_0(\tau) \pm \frac{2}{3}I_1(\tau)) \\ F^{net}(\tau) &= \mu_0(\pi F_0)e^{-\tau/\mu_0} + F^{\downarrow}(\tau) - F^{\uparrow}(\tau) \end{aligned} \tag{13}$$

3.2 Multi layer formalism

The description of the radiative fluxes in a vertical inhomogeneous atmosphere requires to use a multi layer approach. If a vertically inhomogeneous atmosphere is assumed to be subdivided into a finite number N–1 of layers with homogeneous optical properties, we can apply the delta-Eddington solution in each layer:

$$I^i(\tau, \mu) = I_0^i(\tau) + \mu I_1^i(\tau)$$
$$\text{for } \tau_i \leq \tau \leq \tau_{i+1} \qquad i = 1, \ldots, N-1$$

where τ_i and τ_{i+1} are the (scaled) optical depth at the boundaries of layer i. To determine the unknown constants c_1^i and c_2^i of eqs. (8) in each layer i we need $2(N-1)$ boundary conditions. Requiring flux continuity across interior levels we get $2(N-2)$ boundary conditions:

$$\begin{aligned} I_0^i(\tau_{i+1}) &= I_0^{i+1}(\tau_{i+1}) \\ I_1^i(\tau_{i+1}) &= I_1^{i+1}(\tau_{i+1}) \qquad i = 1, \ldots, N-2 \end{aligned} \tag{14}$$

Prescribing a constant diffuse downward flux $F_0^{\downarrow}$ at the top of atmosphere and a constant diffuse upward flux $F_0^{\uparrow}$ as well as Lambert reflection with albedo $A(\mu_0)$ at the bottom we get the two missing boundary conditions:

$$\begin{aligned} F^{\downarrow}(\tau_1 = 0) &= F_0^{\downarrow} \\ F^{\uparrow}(\tau_N = \tau_{max}) &= F_0^{\uparrow} + A(\mu_0)\left[F^{\downarrow}(\tau_N) + \mu_0(\pi F_0)e^{-\tau_N/\mu_0}\right] \end{aligned} \tag{15}$$

Inserting of eqs. (8), (13) in eqs. (14), (15) leads to a set of penta-diagonal linear equations for the unknown constants c_1^i and c_2^i. To get a numerically more stable matrix equation it is better to solve a system of equations not for the bare quantities c_1^i and c_2^i but for $e^{k_i\tau_{i+1}}c_1^i$ and $e^{-k_i\tau_{i+1}}c_2^i$, because these are the quantities needed in eqs. (8) to compute the radiance $I = I_0 + \mu I_1$.

Using the notation of eqs. (8), (9) and

$$\begin{aligned} x_{2i-1} &= e^{-k_i\tau_{i+1}}c_1^i \\ x_{2i} &= e^{k_i\tau_{i+1}}c_2^i \\ e_i &= e^{k_i(\Delta\tau)_i} = e^{k_i(\tau_{i+1}-\tau_i)} \qquad \text{for } i = 1,\ldots,N-1 \end{aligned}$$

we get the following matrix equation

$$\mathbf{M}\,\mathbf{x} = \mathbf{d}_{sw} + \mathbf{d}_{lw}$$

with:

$$\mathbf{M} = \begin{pmatrix} \boxed{(1+p_1)e_1} & \frac{1-p_1}{e_1} & & & & & \\ 1 & \boxed{1} & -e_2 & -\frac{1}{e_2} & & & \\ p_1 & -p_1 & \boxed{-p_2e_2} & \frac{p_2}{e_2} & 0 & & \\ & \ddots & \ddots & \ddots & \ddots & \ddots & \\ & 0 & 1 & \boxed{1} & -e_{i+1} & -\frac{1}{e_{i+1}} & \\ & & p_i & -p_i & \boxed{-p_{i+1}e_{i+1}} & \frac{p_{i+1}}{e_{i+1}} & 0 \\ & & & \ddots & \ddots & \ddots & \ddots \\ & & & 0 & 0 & 0 & 1-A-(1+A)p_{N-1} & \boxed{1-A+(1+A)p_{N-1}} \end{pmatrix} \tag{16}$$

$$\mathbf{d}_{sw} = \begin{pmatrix} F_0^{\downarrow}+\alpha_1+\beta_1 \\ (\alpha_1-\alpha_2)e^{-\tau_2/\mu_0} \\ (\beta_1-\beta_2)e^{-\tau_2/\mu_0} \\ \vdots \\ (\alpha_i-\alpha_{i+1})e^{-\tau_{i+1}/\mu_0} \\ (\beta_i-\beta_{i+1})e^{-\tau_{i+1}/\mu_0} \\ \vdots \\ F_0^{\uparrow}+(\alpha_{N-1}-\beta_{N-1}+A(\mu_0(\pi F_0)-\alpha_{N-1}-\beta_{N-1}))e^{\tau_N/\mu_0} \end{pmatrix} \tag{17}$$

$$\mathbf{d}_{lw} = \begin{pmatrix} F_0'^{\downarrow} - \pi B(\tau_1) + \frac{2\pi}{3(1-\omega_1 g_1)} \frac{\partial B}{\partial \tau}\Big|_1 \\ 0 \\ \frac{1}{1-\omega_1 g_1} \frac{\partial B}{\partial \tau}\Big|_1 - \frac{1}{1-\omega_2 g_2} \frac{\partial B}{\partial \tau}\Big|_2 \\ \vdots \\ 0 \\ \frac{1}{1-\omega_i g_i} \frac{\partial B}{\partial \tau}\Big|_i - \frac{1}{1-\omega_{i+1} g_{i+1}} \frac{\partial B}{\partial \tau}\Big|_{i+1} \\ \vdots \\ \\ \\ F_0'^{\uparrow} - (1+A) \frac{2\pi}{3(1-\omega_{N-1} g_{N-1})} \frac{\partial B}{\partial \tau}\Big|_{N-1} \end{pmatrix} \tag{18}$$

The vector $\mathbf{d}_{sw}$ contributes to the right side of eq. (16), if the solar input (πF_0) is not zero i.e. in the shortwave region, where the Planck radiation and thus the vector $\mathbf{d}_{lw}$ has no considerable contribution. In the longwave region $\mathbf{d}_{lw}$ is the only contribution to the right side of eq. (16).

The matrix $\mathbf{M}$ eq. (16) is similar to that of Wiscombe (1977). But there is a substantial difference in terms of numerical stability. Ill-conditioning of the matrix $\mathbf{M}$ can occur when the main diagonal[1] is dominated by the second or even worse by the third diagonal. In this context a high optical depth in one or more layers is critical because then $e_i = e^{k_i(\Delta\tau)_i} \gg 1$. Then the entry in the main diagonal of the rows with even numbers is dominated by the entry of the upper second diagonal. In contrast to the matrix given by Wiscombe (1977) the matrix $\mathbf{M}$ is never dominated by the third diagonal and in the rows with odd numbers the main diagonal dominates or is in the same order as the second and third diagonals for all possible values of p_i, e_i.

To find the solution of the matrix equation an algorithm as simple as possible should be used. If this algorithm is independent of the details of eq. (16), i. e. of the given optical properties, we can solve eq. (16) with a minimum of computing steps. In addition we can compute the radiative transfer for a number of vertical columns simultaneously. This leads to an optimal performance on a vector computer and allows an online use of the delta-Eddington method in a regional or global climate model. A commonly used method to solve matrix equations is a standard L-U (lower triangular, upper triangular) decomposition of a row-wise permutation of $\mathbf{M}$, arrived at by row equilibration and partial pivoting. This method is reliable and numerically quite stable, but requires a lot of computing steps and prevents the desirable simultaneous computation of a number of vertical columns. The fastest direct method to solve a matrix in pentadiagonal form is a simple gaussian algorithm. This algorithm is independent of the matrix entries, needs only six computing steps for each row for the matrix transformation (i. e. twelve steps per atmospheric layer) and allows for a simultaneous solution of many vertical columns.

A gaussian algorithm for solving eq. (16) can only be used if ill-conditioning is avoided for all possible input quantities. To avoid the already mentioned ill-conditioning for high optical depth an improvement is achieved just by adding the negative of each odd row to the even row above. Then the ratio of main diagonal to the upper second diagonal is always greater than before, in the case of pure absorption ($\omega = 0$) by more than one order of magnitude. Another case of ill-conditioning arises from the fact that in the case of high optical depths the entries of the main diagonal vary from line to line by many orders of magnitude. By simply normalizing the main diagonal to one this case of ill-conditioning is avoided.

If a 64 bit arithmetical precision on the computer system[2] is used the achieved matrix equation is numerically stable enough that a simple gaussian algorithm can be used to find the correct

[1] marked with boxes in (16)

[2] 64 bit arithmetic is single precision on our Cray C90-system and double precision on normal workstations

solution. To handle the case of high optical depth there is no restriction necessary except that the exponential expressions in matrix M must be a finite number for the computing system:

$$e_i = e^{k_i(\Delta\tau)_i} < \infty \qquad \Rightarrow \qquad k_i(\Delta\tau)_i < 700. \tag{19}$$

In the case of pure absorbing ($\omega_i = 0 \Rightarrow k_i = 2/\sqrt{3}$) this leads to a maximum optical depth for each layer of six hundred. In the case of additional scattering the restriction is weakened. This is a substantial improvement compared to other authors. E. g. Wiscombe (1977) requires $k_i(\Delta\tau)_i < 14$ which for pure absorbing corresponds to a maximum optical depth for each layer of ten.

A comparable restriction must be applied for the vector $\mathbf{d}_{sw}$:

$$e^{\tau_i/\mu_0} < \infty \qquad \Rightarrow \qquad \tau_i/\mu_0 < 700. \tag{20}$$

This means a restriction not only for the optical depth of a single layer but also for the total optical depth of the vertical column.

If Planck radiation is present i. e. $\mathbf{d}_{lw}$ is not zero, a minimal optical depth for each layer is required:

$$B(\tau_i) \ll \frac{2}{3(1-\omega_i g_i)} \frac{\partial B}{\partial \tau}\Big|_i \qquad \Rightarrow \qquad \Delta\tau_i > 10^{-12} \tag{21}$$

If the restrictions (19) - (21) to the input quantities for the matrix equation (16) are applied , the described fast algorithm is reliable for all values of optical input data. Thus the delta-Eddington model in a multi layer formalism offers the possibility to compute the monochromatic radiative transfer in any vertically inhomogeneous atmosphere. For the use of the described radiative transfer scheme in climate models it is necessary to perform an integration over wavelengths, i. e. wavelength intervals and optical properties must be determined in an appropriate manner.

3.3 Optical properties

Only the shortwave part of the solar spectrum (0.2 to 5.0 μm) subdivided into 18 wavelength intervals is considered until now in the radiation transfer model. Unequal spectral interval length as well as spectral data for important absorbers (ozone, water vapour, oxygen and carbon dioxide) and scatterers, in particular clouds, is taken from Briegleb (1992). This parameterization explicitly relates cloud radiative properties to cloud droplet properties (liquid water path and effective radius). The simple and efficient method to simulate partial cloud cover and cloud overlap is also taken from Briegleb (1992).

Optical properties of the dry sulfate aerosol were determined by Schult (personal communication) from Mie theory calculations, assuming a zero order logarithmic size distribution with a mean particle radius of 0.05 μm and a geometric standard deviation of 1.8. In addition, the particle density was set to 1.6 gcm^{-3} for an aerosol mixture of 75% H_2SO_4 and 25% H_2O. The resulting wavelength dependent values for specific extinction, single scattering albedo and asymmetry parameter are given in Tab. 1. These values agree almost perfectly with the data given by Kiehl and Briegleb (1993), except the specific extinction for wavelength smaller than 1.0 μm (our estimate is about 0.75 times the specific extinction based on Kiehl and Briegleb (1993)). In order to consider the modification of the aerosol specific extinction due to the influence of the relative humidity of the ambient air, we use a simple approximation adopted from the data given by Nemesure et al. (1995). If the relative humidity RH is less than 80%, the specific extinction is enhanced by a factor of RH *0.04, assuming a minimum relative humidity of 25%. For relative humidity exceeding 80%, the specific extinction increases exponentially with RH until a factor of 9.9 is reaches at RH = 100%. Relating aerosol specific extinction at 80% relative humidity to 50% results in a factor 1.6, which is in good agreement with the relative humidity factor 1.7 determined by Charlson et al. (1991).

The indirect radiative forcing of sulfate aerosol is determined from an empirical relationship between sulfate aerosol mass concentration M_{sulf} and cloud droplet number concentration CDNC (Boucher and Lohmann, 1995, relationship D)

$$CDNC = 0.162 \cdot 10^9 \cdot (M_{sulf})^{0.41} \tag{22}$$

CDNC is then related to the droplet effective radius r_e

$$r_e = 1.1 \cdot \left(\frac{3}{4\Pi} \cdot \frac{L \cdot \rho air}{\rho water \cdot CDNC \cdot FRAC} \right) \tag{23}$$

with L as liquid water content and FRAC as fractional cloud cover. Thus, varying cloud radii are explicitly used to estimate the indirect effect of sulfate aerosols on cloud reflectance. As for the indirect shortwave forcing the total sulfate effect is unknown (i.e. we do not know how clouds behave without any CDNC in the atmosphere), only the indirect effect of anthropogenic sulfate can be determined. This was done by running the radiative transfer model once with the total sulfate load and once with the natural sulfate load only. Subtracting the latter one gives the indirect shortwave forcing of anthropogenic sulfate.

3.4 Input data

Besides the information directly related to sulfate aerosols (mass distribution, relative humidity and effective cloud droplet radius), the radiation transfer model needs input about the physical conditions of the atmosphere (pressure, density, specific humidity, liquid water content, cloud cover and surface albedo). In addition, ozone concentrations have to be specified. In a first attempt we included standard atmosphere ozone concentrations.

4. Model simulation and results

The regional model system HIRHAM-CTM, described in section 2, was run for one winter (January, 13-23, 1991) and one summer episode (July, 23-30, 1990). Validation and sensitivity studies of these episodes are described in Langmann (1995).

To emphasize the capability of the high resolution regional model to resolve small scale patterns of the shortwave sulfate forcing, which are smoothed out by coarse grid models, a qualitative comparison to global model results is shown. For this purpose a five year run with the global climate model ECHAM (T30 resolution $\cong 3.75°$) including the tropospheric sulfur cycle (Feichter et al., 1996) with source marked sulfur species (Graf et al., 1996) has been chosen. This study allows to distinguish between sulfate from DMS, volcanoes, biomass burning and anthropogenic origin. It should be stressed here that regional and global model results are only compared in a qualitative way due to the episodic versus long-term nature of the experiments. As results episodic mean and monthly mean values of the 5 year run are shown. The radiative transfer model described in section 3 is applied to both scales as "off-line" analysis tool to determine the direct and indirect top of atmosphere forcing of sulfate aerosols. This was possible in a straightforward manner, because the global and the regional model use the same vertical hybrid pressure-sigma coordinate system.

4.1. Summer simulation

The global model predicts a European total sulfate burden of 49.6 Gg S which exceeds the regional model prediction by about 8 Gg S. The European vertical profiles for total sulfate and anthropogenic sulfate are shown in Figure 1. Here the anthropogenic sulfate fraction of the regional model simulation is crudely estimated for comparison by subtracting the initial sulfate profile from the episodic mean, because no information about the source type of sulfate particles is included in HIRHAM-CTM. In the PBL the anthropogenic contribution to the European sulfate burden is highest. When comparing modelled and measured surface atmospheric concentrations, the natural contribution is negligible. This is different if one looks at deposition fields (Mcardle et al., 1995). In the free troposphere sulfate from natural sources (volcanoes and DMS) dominates. Hence, in the global model simulation 54% of the European total sulfate burden in July are of natural origin. As already mentioned in section 2, chemical species concentrations in HIRHAM-CTM are initialized with estimated horizontally uniform vertical profiles of a clean atmosphere. These profiles also serve as fixed boundary conditions. This assumption is justified, if the lateral model boundaries are far away from source regions and if only a small temporal variability is expected. But as shown in Figure 1 the initial sulfate burden makes up an important fraction of the total sulfate burden (33% in summer, 56% in winter). A future perspective to test the sensibility of a model simulation to chemical initial and boundary conditions could be a chemical nesting procedure of the limited area model into the global model. Thus a

more realistic initial distribution of chemical species - for example from nudged model runs - would be available as well as a possible temporal variability in concentration fields at the model boundaries.

The prediction of a higher European total sulfate burden by the global model in July leads to a higher European mean top of atmosphere direct forcing of sulfate aerosols in comparison to the regional model results (Figure 2). In addition, the global model calculates a smaller cloud cover over Europe in the summer month, strengthening the difference between regional and global prediction of the direct shortwave radiative sulfate forcing. Looking at the clear sky direct forcing of sulfate aerosols (Figure 3), the cloud effect is switched off. In this case differences in the regional and global model simulation are produced mainly by differences in the total sulfate burden and, of course, the horizontal resolution. The frame in Figure 2a and Figure 3a marks that part of Europe, which is also covered by the regional model. It is interesting to note that the spatial pattern of the solar radiative sulfate forcing is very similar in both models with a minimum forcing over Southern Spain and Portugal and a band of maximum forcing from the south-east corner to the north-west corner of the regional model area. The radiative effect of natural sulfate over Europe in the global model calculation is significantly smaller (34%) than its contribution to the sulfate burden (54%). This figure is due to the distribution of natural sulfate in higher altitudes, where the ambient humidity leads to a smaller increase of the aerosol specific extinction than in the planetary boundary layer, where most of the anthropogenic sulfate is located.

Calculating the indirect forcing of anthropogenic sulfate aerosols for July (Figure 4), a rather homogeneous forcing field is determined by the global model and a very patchy one by the regional model. In this case the high spatial and temporal variability of cloud fields is directly reflected in the episodic mean of the regional model indirect forcing, whereas the long term average of the coarse grid global model simulation results in a smoothed forcing field. However, the main contribution to the indirect forcing of anthropogenic sulfate aerosols is located between 50° and 65° north in both model simulations. More clouds over Europe in the regional model calculation and the estimated higher anthropogenic SO_4^{2-} burden (Figure 1) are responsible for the enhanced indirect solar European sulfate forcing in comparison to the global model simulation.

4.2. Winter simulation

The total sulfate burden (Figure 1) is much smaller in winter than in summer for both model scales over Europe, because in winter oxidation of SO_2 is slower and wet deposition of SO_4^{2-} is very efficient. The seasonal differences occur mainly at the top of the PBL, whereas the atmospheric near surface sulfate burden remains unchanged. Anthropogenic sulfate makes up 62% of the total European sulfate burden in winter, and only 46% in summer. The reason is the seasonally dependent DMS emission from the oceans, which is negligible in winter.

Although a very good agreement of the total European sulfate burden is predicted by both models in the winter simulations, the direct shortwave sulfate forcing is very different (Figure 5). The regional model prediction is about two times the global one in the European mean. Nearly no forcing is determined north of 55° by the regional model, the global model predicts a negligible forcing north of 45°. Due to the higher horizontal resolution, the regional model shows

smaller scale phenomena, like the influence of the high surface albedo of the snow covered Alps. Additional sulfate has no large backscattering effect there. The global model does not resolve this feature. The result is a smoothed forcing pattern. As already mentioned for the summer simulation, different cloud cover predictions by the regional and the global model modify the forcing significantly. In winter the global model determines more clouds over Europe, thus reducing the direct shortwave sulfate forcing in comparison to the regional model results. Switching off the occurrence of clouds in the radiation transfer calculation, the clear sky direct forcing of sulfate is obtained (Figure 6), which shows better agreement on both model scales. The smaller amount of anthropogenic sulfate aerosols over Europe in January (Figure 1) together with the smaller cloud cover in the regional model simulation results in an indirect solar European forcing of anthropogenic sulfate aerosols, which is significantly below the global model prediction (Figure 7).

5. Summary and conclusions

A computationally efficient and stable method of the delta-Eddington approximation for a multi layer atmosphere has been presented, which allows to include additional scatteres like aerosols in a straight forward manner. It was applied in this study and in Graf et al. (1996) as off-line analysis tool. For the application of this radiation model as part of a regional or global circulation model the longwave part of the spectrum should be included. Here it was used to determine the direct and indirect shortwave radiative effect of sulfate aerosols as simulated by a modified version of the regional chemistry-transport-model of the EURAD system and the global chemistry-circulation model ECHAM. Regional and global model results are comparable concerning the distribution and amount of sulfate burden and radiative forcing over Europe, despite the episodic and long term integration time of the respective experiments. However, different cloud cover prediction by the regional and global model modifies the forcing significantly. As expected, the regional model shows smaller scale phenomena due to the higher horizontal resolution, which cannot be resolved by the global model. Natural sources (DMS and volcanoes) contribute significantly to the European sulfate budget and shortwave radiative forcing. Hence, the initial and boundary chemical composition of the atmosphere for the limited area model should be investigated in more detail in the future.

References:

Boucher, O. and T.L. Anderson (1995): General circulation model assessment of the sensitivity of direct climate forcing by anthropogenic sulfate aerosols to aerosol size and chemistry. *J. Geophys. Res.*, **100**, 26,117-26,134.

Boucher, O. and U. Lohmann (1995): The sulfate-CCN-cloud albedo effect, a sensitivity study with two general circulation models. *Tellus*, **47 B**, 281-300.

Briegleb, B.P. (1992): Delta-Eddington Approximation for Solar Radiation in the NCAR Community Climate Model. *J. Geophys. Res.*, **97**, 7603-7612.

Chang, J.S., R.A. Brost, I.S.A. Isaksen, S. Madronich, P. Middleton, W.R. Stockwell and C.J. Walcek (1987): A three-dimensional Eulerian acid deposition model: physical concepts and formulation. *J. Geophys. Res.*, **92**, 14,681-14,700.

Charlson, R.J., J. Langner, H. Rodhe, C.B. Leovy and S.G. Warren (1991): Pertubation of the northern hemisphere radiative balance by backscattering from anthropogenic sulfate aerosols. *Tellus*, **43 AB**, 152-163.

Feichter, J., E. Kjellstrom, H. Rodhe, F. Dentener, J. Lelieveld and G.-J. Roelofs (1996): Simulation of the tropospheric sulfur cycle in a global climate model. *Atm.. Environ.*, **30**, 1693-1707.

Fouquart, Y. and B. Bonnel (1980): Computations of solar heating of the earth´s atmosphere: a new parameterization. *Beitr. Phys. Atmos.*, **53**, 35-62.

Graf, H.-F., J. Feichter and B. Langmann (1996): Volcanic sulfur emissions: Estimate of source strength and its contribution to the global sulfate distribution, accepted by *J. Geophys. Res.*

Hass, H. (1991): Description of the EURAD Chemistry-Transport-Model version 2 (CTM2) (edited by Ebel, A., F.M. Neubauer and P. Speth). Report 83, Institute of Geophysics and Meteorology, University of Cologne.

Hasselmann, K., Bengtsson, L., Cubasch, U., Hegerl G.C., Rodhe, H., Roeckner, E., von Storch, H., Voss, R. and Waszkewitz, J. (1995): Detection of anthropogenic climate change using a fingerprint method. MPI Report, **168** and Proc. "Modern Dynamical Meteorology", Symposium in Honor of Aksel Wiin-Nielsen, 1995. ed. P. Ditlevsen (ECMWF press 1995), 203-221.

IPCC, Climate Change 1995, The science of climate change. Intergovernmental Panel of Climate Change, J.T. Houghton, L.G.M. Filko, B.A. Callander, N. Narris, A. Kattenberg and K. Maskell (Eds.). Cambridge University Press, Cambridge, U.K. 572 pp. (1996).

Kållberg, P. (1989): The HIRLAM forecast model level 1 documentation manual. SMHI, S-60176 Norrköping, Sweden.

Kiehl, J.T. and B.P. Briegleb (1993): The relative roles of sulfate aerosols and greenhouse gases in climate forcing. *Science*, **260**, 311-314.

Langmann, B. (1995): Incorporation of the regional tropospheric chemistry in the Hamburg climate model system: Model calculations and comparison with observations. Ph.D. Thesis No. 29, Max-Planck-Institut für Meteorologie, Hamburg, Germany. In German.

Langmann, B. and H.-F. Graf (1996): The chemistry of the polluted atmosphere over Europe: Simulations and sensitivity studies with a regional Chemistry-Transport-Model. Accepted by *Atmos. Environ.*

Madronich, S. (1987): Photodissociation in the atmosphere. I: Actinic flux and the effect of ground reflections and clouds. *J. Geophys. Res.*, **92**, 9,740-9,752.

Mcardle, N.C., G.W. Campbell and J.R. Stedman (1995): Wet deposition of the non sea-salt sulphate in the United Kingdom: The influence of natural sources. *Water, Air and Soil Pollution* ,**85**, 1941-1948.

Memmesheimer, M., J. Tippke, A. Ebel, H. Hass, H.J. Jakobs and M. Laube (1991): On the use of EMEP emission inventories for European scale air pollution modelling with the EURAD model. EMEP Workshop on Photooxidant Modelling for long-range Transport in Relation to Abatement Strategies. Berlin, Germany, 16-19 April 1991, pp. 307-324.

Mitchell, J.F.B., T.C. Johns, J.M Gregory and S.F.B. Tett (1995): Climate response to increasing levels of greenhouse gases and sulfate aerosols. *Nature,* **376**, 501-504.

Mölders, N. and M. Laube (1994): A numerical study on the influence of different cloud treatment in a chemical transport model on gas phase distribution. *Atmos. Res.,* **32**, 249-272.

Nemesure, S., R. Wagner and S.E. Schwartz (1995): Direct shortwave forcing of climate by the anthropogenic sulfate aerosol: sensitivity to particle size, composition and relative humidity. *J. Geophys. Res.,* **100**, 26,105-26,116.

Pilinis, C., S.N. Pandis and J.H. Seinfeld (1995): Sensitivity of direct climate forcing by atmospheric aerosols to aerosol size and composition. *J. Geophys. Res.,* **100**, 18,739-18,754.

Roeckner, E., T. Siebert and J. Feichter (1995): Climate response to anthropogenic sulfate forcing simulated with a general circulation model. Dahlem Workshop on Aerosol Forcing of Climate (Eds.: R.J. Charlson and J. Heintzenberg), Wiley & Sons, pp. 349-362.

Roeckner, E., K. Arpe, L. Bengtsson, M. Christoph, M. Claussen, L. Duemenil, M. Esch, M. Giorgetta, U. Schlese and U. Schulzweida (1996): The atmospheric general circulation model ECHAM-4: Model description and simulation of present-day climate. MPI Report No. 218. Sept. 1996.

Smolarkiewitz, P.K. (1983): A simple positive definite advection scheme with small implicit diffusion. *Mon. Weather Rev.,* **111**, 479-486.

Stockwell, W.R., P. Middleton, J.S. Chang and X. Tang (1990): The second generation regional acid deposition model: Chemical mechanism for regional air quality modelling. *J. Geophys. Res.,* **95**, 16,343-16,367.

Taylor, K. and J.E. Penner (1994): Response of the climate system to atmospheric aerosols and greenhouse gases. *Nature,* **369**, 734-737.

Wesely, M.L. (1989): Parameterization of surface resistances to gaseous dry deposition in regional-scale numerical models. *Atmos. Environ.* **23**, 1293-1304.

Wigley, T.M.L. and S.C.B. Raper (1990): Natural variability of the climate system and detection of the greenhouse effect. *Nature*, **344**, 324-327.

Wiscombe, W.J. (1977): The Delta-Eddington Approximation for a Vertically Inhomogeneous Atmosphere. NCAR/TN-121+STR, Boulder, Colorado, U.S.A.

Figures:

Figure 1: European total and anthropogenic vertical sulfate distribution as determined by the global and regional chemistry-circulation model for January and July.

Figure 2: Direct shortwave forcing of total sulfate in July,
a) global model prediction, b) regional model prediction.

Figure 3: Clear sky direct shortwave forcing of total sulfate in July,
a) global model prediction, b) regional model prediction.

Figure 4: Indirect shortwave forcing of anthropogenic sulfate in July,
a) global model prediction, b) regional model prediction.

Figure 5: As Figure 2, but for January.

Figure 6: As Figure 3, but for January.

Figure 7: As Figure 4, but for January.

Table 1: Optical properties of the dry sulfate aerosol as function of the applied wavelength intervals

Interval	min [a]	max [b]	E [c]	g [d]	ω [e]
1	0.200	0.245	5.7	0.7	1
2	0.245	0.265	5.5	0.7	1
3	0.265	0.275	5.4	0.7	1
4	0.275	0.285	5.3	0.7	1
5	0.285	0.295	5.1	0.7	1
6	0.295	0.305	5.0	0.7	1
7	0.305	0.350	4.7	0.7	1
8	0.350	0.700	3.5	0.72	1
9	0.700	1.190	2.2	0.7	1
[f] 10	1.190	2.380	0.86	0.63	0.99
11	1.190	2.380	0.86	0.63	0.99
12	1.190	2.380	0.86	0.63	0.99
13	1.190	2.380	0.86	0.63	0.99
[f] 14	2.380	4.000	0.28	0.47	0.48
15	2.380	4.000	0.28	0.47	0.48
16	2.630	2.860	0.29	0.49	0.49
[f] 17	4.160	4.550	0.25	0.36	0.18
18	4.160	4.550	0.25	0.36	0.18

a) Interval minimum wavelength in μm
b) Interval maximum wavelength in μm
c) specific extinction in m^2/g
d) asymmetry factor
e) single scattering albedo
f) the repetition of interval 10, 14 and 17 is caused by the approach of Briegleb (1992) to handle cloud scattering and absorption and CO_2 absorption

Fig. 1

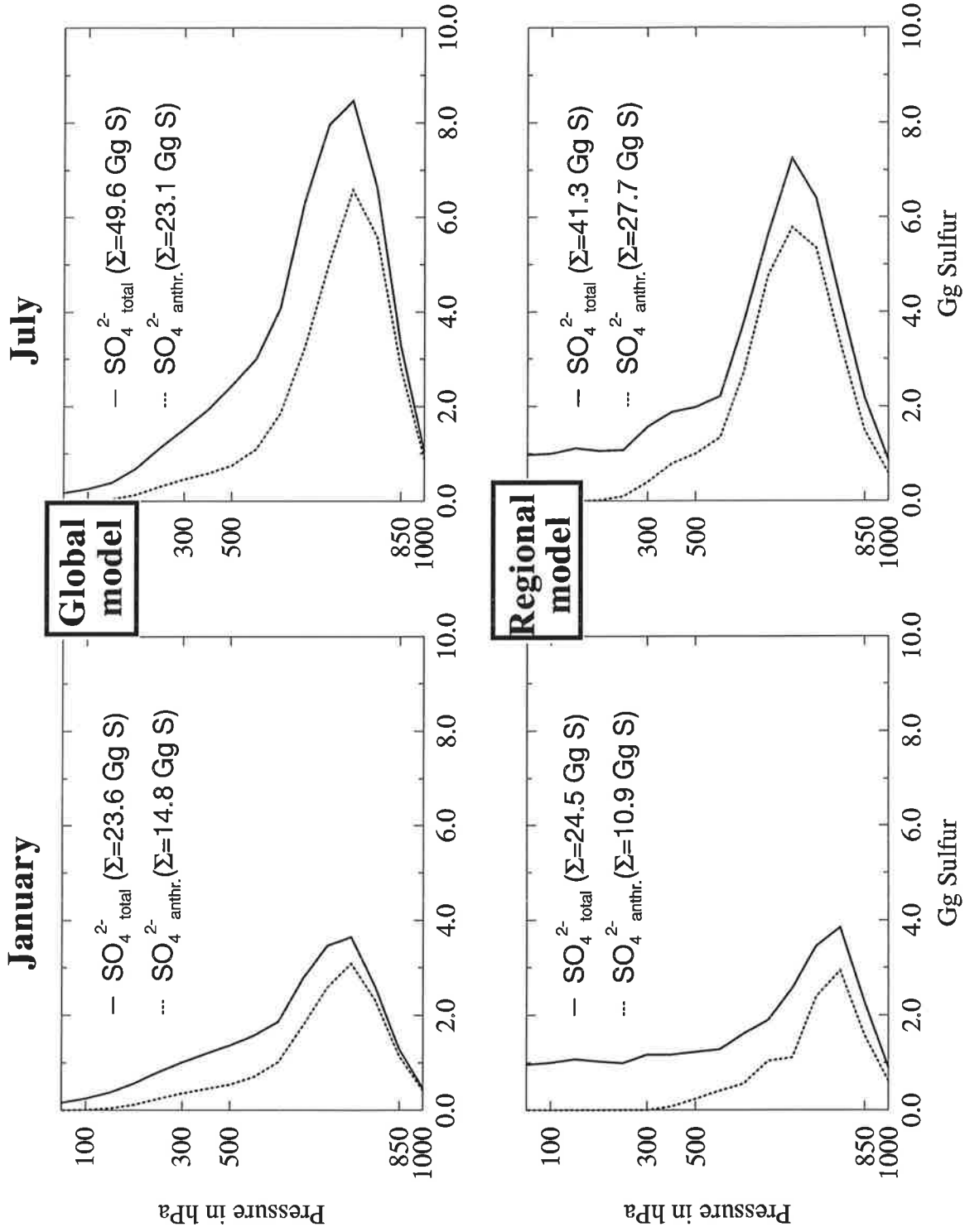
January
July
Global model
Regional model
Pressure in hPa
Gg Sulfur
100
300
500
850
1000
0.0
2.0
4.0
6.0
8.0
10.0
— SO_4^{2-} total (Σ=23.6 Gg S)
··· SO_4^{2-} anthr. (Σ=14.8 Gg S)
— SO_4^{2-} total (Σ=49.6 Gg S)
··· SO_4^{2-} anthr. (Σ=23.1 Gg S)
— SO_4^{2-} total (Σ=24.5 Gg S)
··· SO_4^{2-} anthr. (Σ=10.9 Gg S)
— SO_4^{2-} total (Σ=41.3 Gg S)
··· SO_4^{2-} anthr. (Σ=27.7 Gg S)

Fig. 2

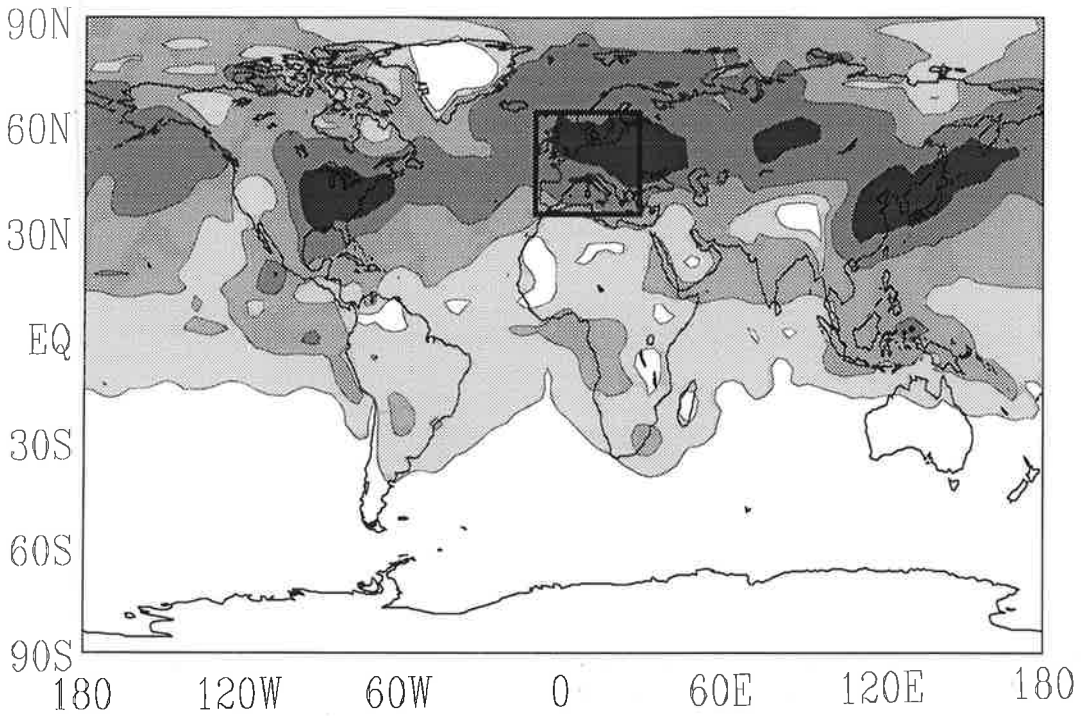

a)

European anthropogenic contribution: 66%

European mean: -3.6 W/m^2 European max: -7.1 W/m^2

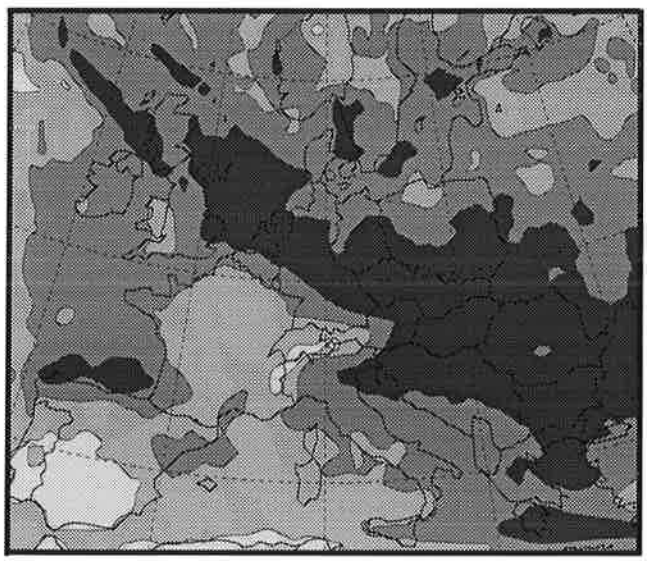

b)

mean: -3.0 W/m^2 max: -9.7 W/m^2

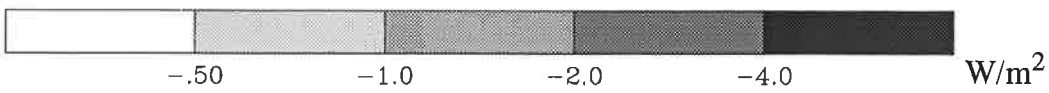

Direct forcing of sulfate aerosols in July

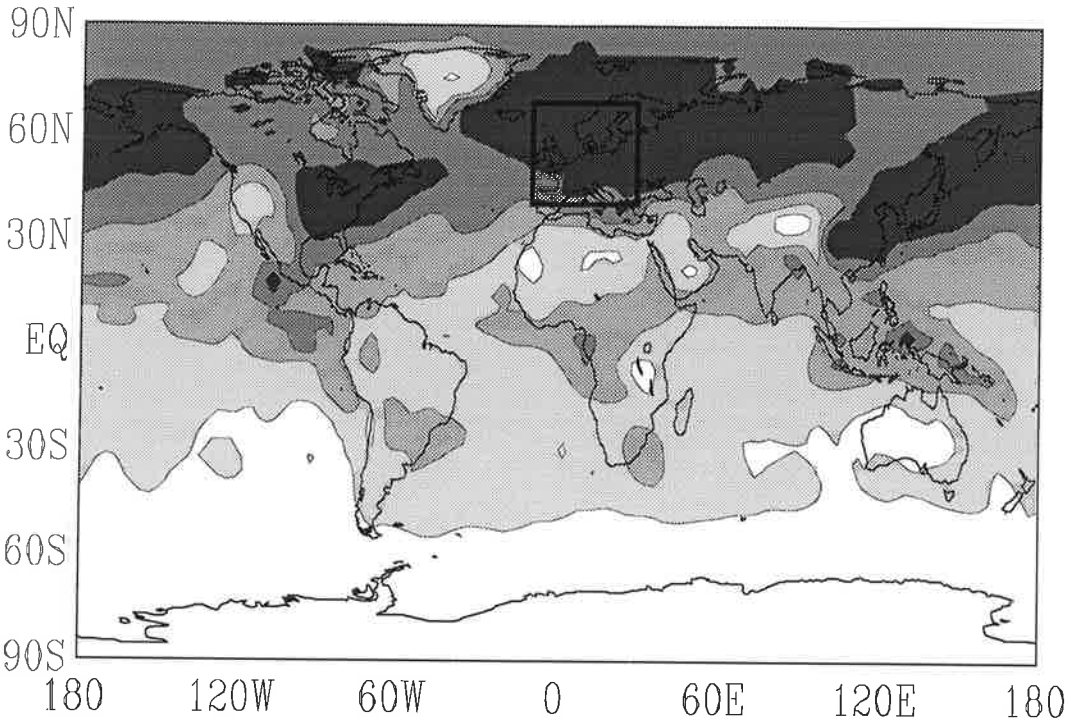

a)

European anthropogenic contribution: 68 %

European mean: -5.4 W/m^2 European max: -1.26 W/m^2

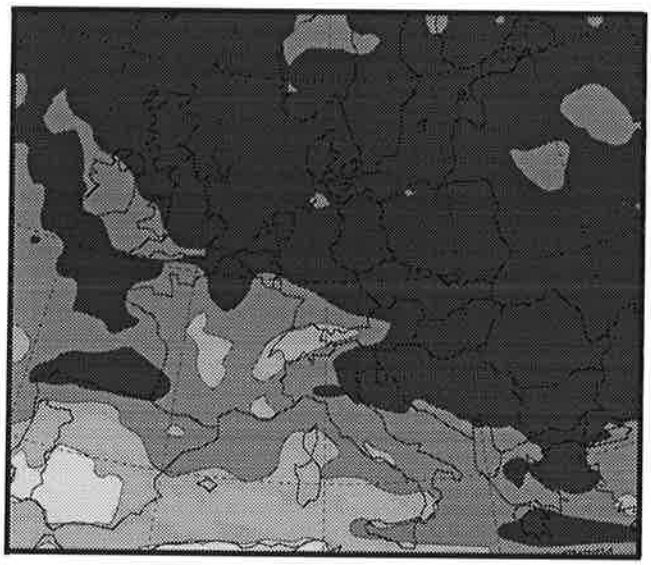

b)

mean: -4.7 W/m^2 max: -17.3 W/m^2

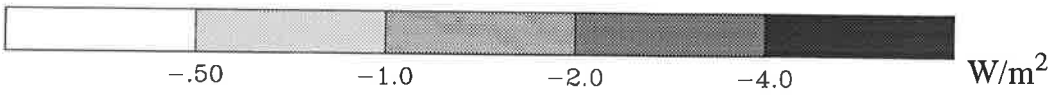

Clear sky direct forcing of sulfate aerosols in July

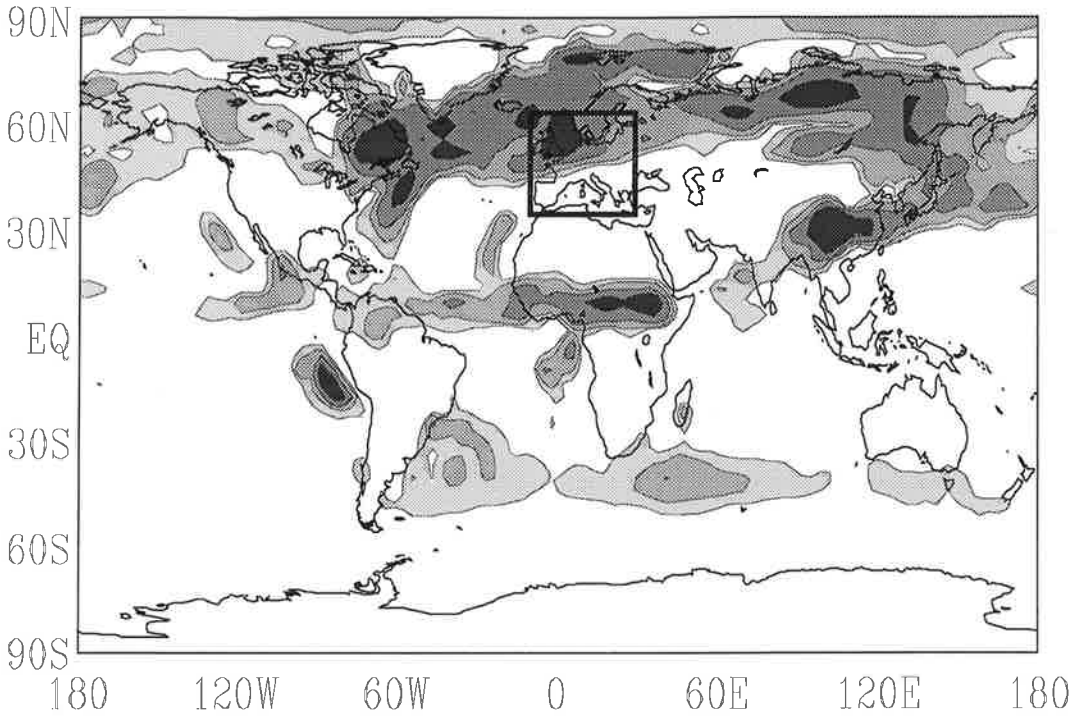

a)

European mean: -1.7 W/m^2 European max: -6.5 W/m^2

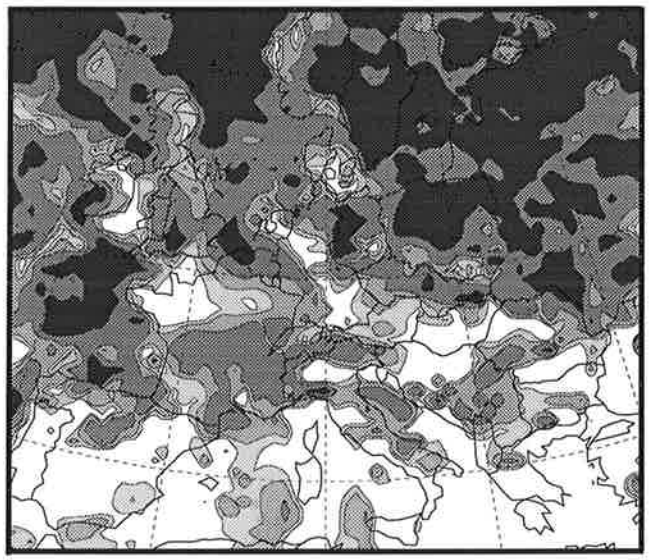

b)

mean: -2.5 W/m^2 max: -11.8 W/m^2

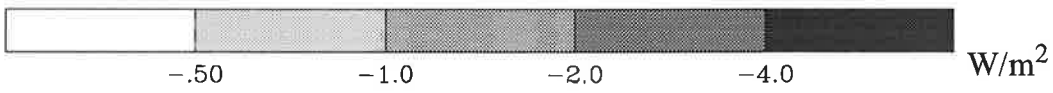

Indirect forcing of anthropogenic sulfate aerosols in July

Fig. 5

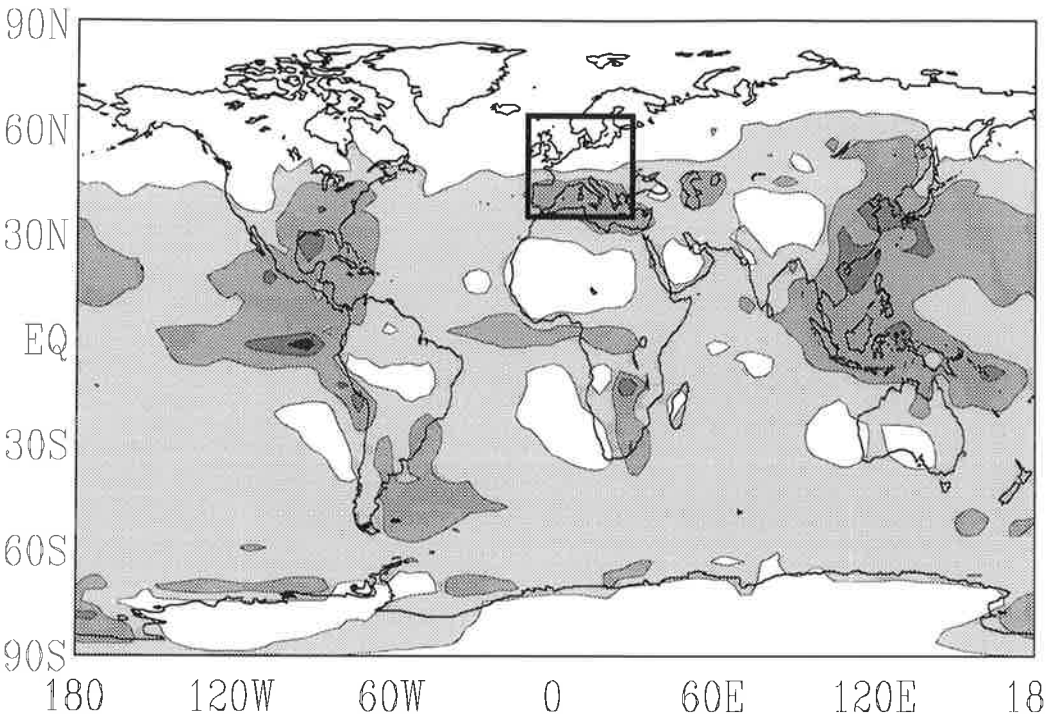

a)

European anthropogenic contribution: 72 %

European mean: -0.57 W/m^2 European max: -1.8 W/m^2

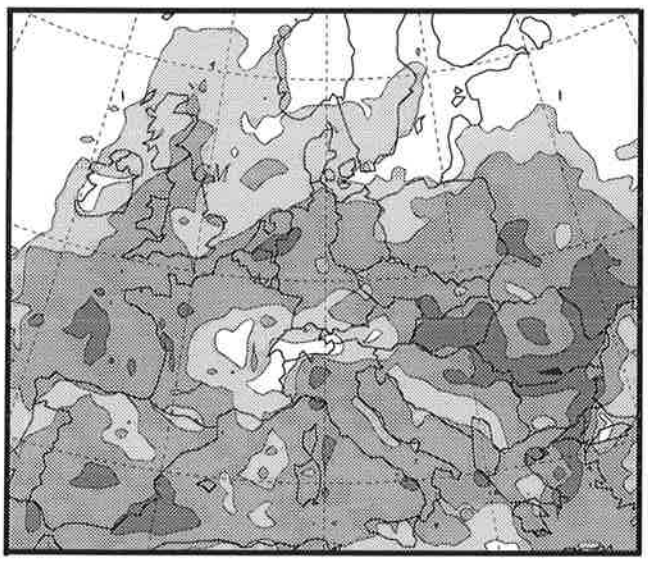

b)

mean: -1.1 W/m^2 max: -4.3 W/m^2

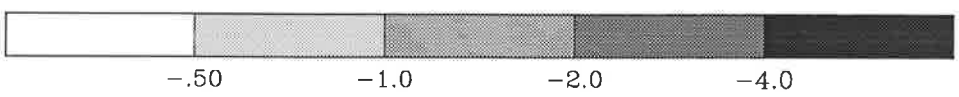

Direct forcing of sulfate aerosols in January

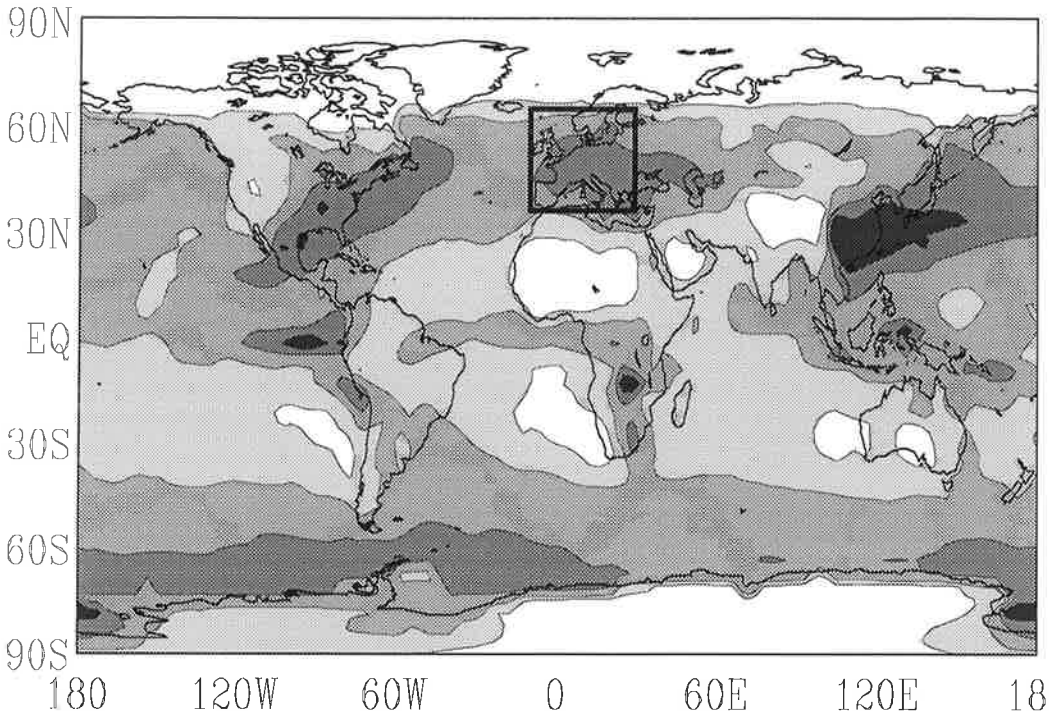

b)

European anthropogenic contribution: 76 %

European mean: -1.9 W/m^2 European max: -3.9 W/m^2

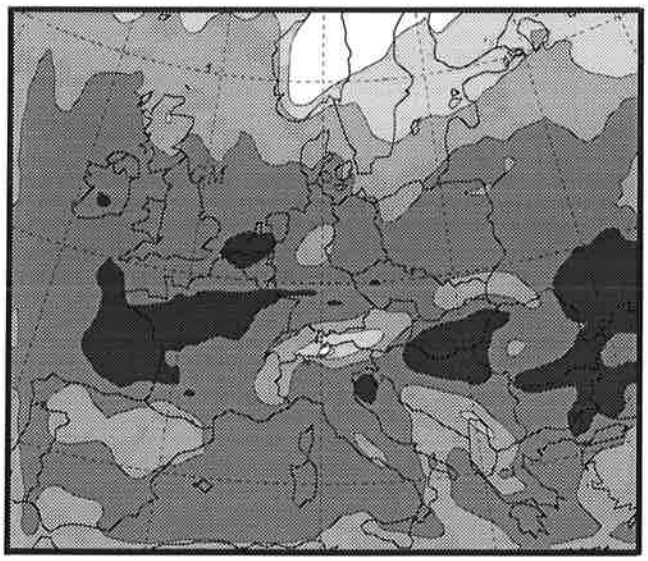

a)

mean: -2.4 W/m^2 max: -6.0 W/m^2

W/m^2

Clear sky direct forcing of sulfate aerosols in January

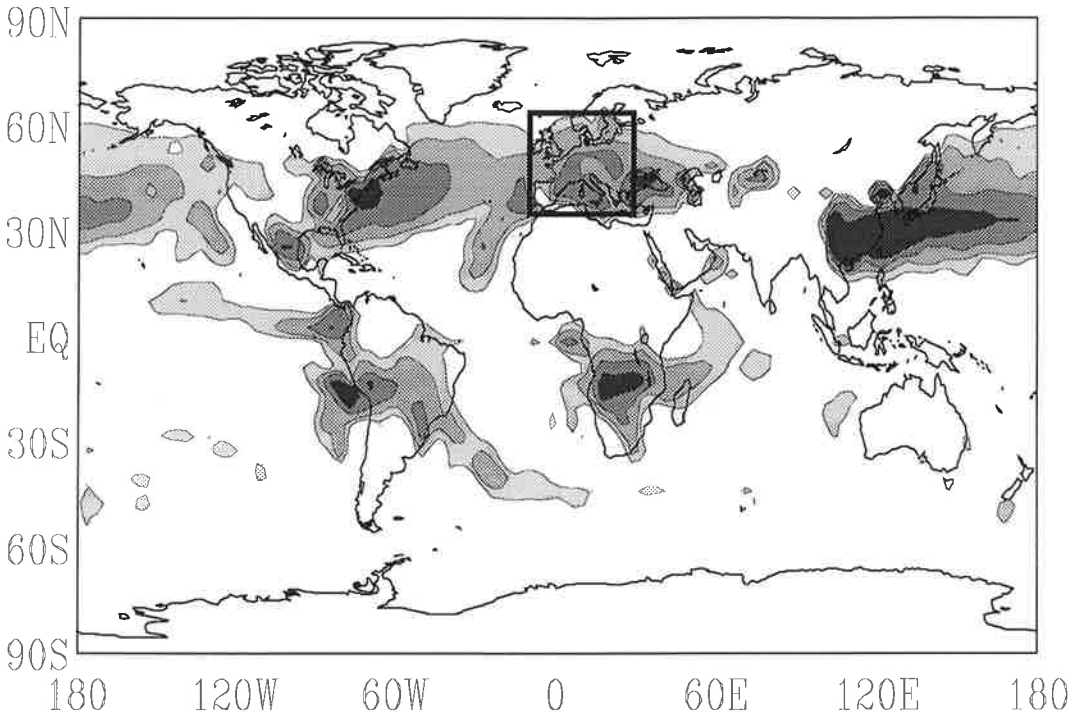

a)

European mean: -1.4 W/m^2 European max: -5.2 W/m^2

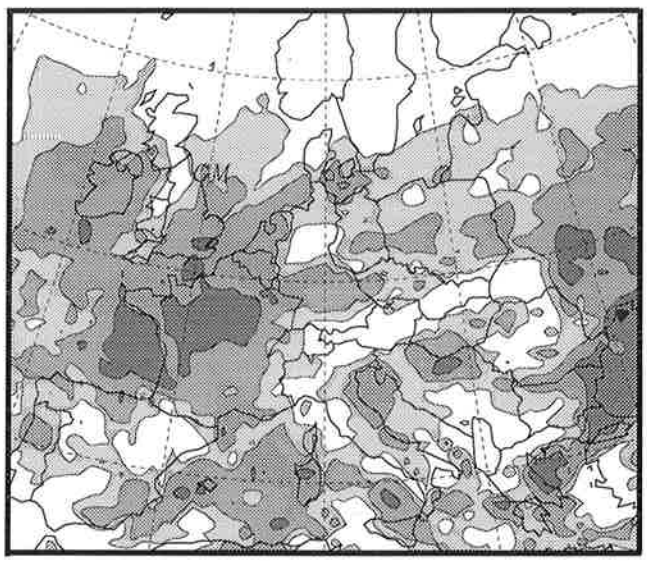

b)

mean: -0.85 W/m^2 max: -4.5 W/m^2

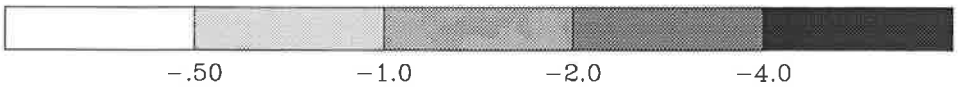

Indirect forcing of anthropogenic sulfate aerosols in January